Optical Fiber Technology 33 (2017) 71–76

Contents lists available at ScienceDirect

Optical Fiber Technology

www.elsevier.com/locate/yofte

Regular Articles

Refractive index sensor based on tapered multicore fiber

Chuanbiao Zhang, Tigang Ning, Jing Li *, Li Pei, Chao Li, Heng Lin

Key Lab of All Optical Network & Advanced Telecommunication Network of EMC, Beijing Jiaotong University, Beijing 100044, China

ARTICLE INFO

Article history:
Received 24 March 2016
Accepted 6 November 2016
Available online 18 November 2016

Keywords:
Fiber optics sensors
Refractive index
Multicore fiber

ABSTRACT

A novel refractive index (RI) sensor based on middle-tapered multicore fiber (TMCF) is proposed and experimentally demonstrated. The sensing structure consists of two singlemode fibers (SMF) and simply spliced a section tapered four-core fiber between them. The light injected from the SMF into the multicore fiber (MCF) will excite multiple cladding mode, and interference between these modes can be affected by the surrounding refractive index (SRI), which also dictates the wavelength shift of the transmission spectrum. Our experimental investigations achieved a sensitivity around 171.2 nm/RIU for a refractive index range from 1.3448 to 1.3774. All sensors fabricated in this paper show good linearity in terms of the spectral wavelength shift versus changes in RI.

1. Introduction

Due to numerous advantages over electronic based sensors, such as immunity to electromagnetic interference, compact size, low cost, remote sensing capability and linear response, optical fiber sensors have been developed in multi-field applications, like structural monitoring [1,2], high temperature sensing [3,4] and biosensors [5,6].

In previous work, there are a number of approaches have been proposed to implement RI sensing, which precisely is the key to achieving bio-photonic sensing. Tapered fiber is one of the commonly used technologies of refractive index sensors [7–13]. Such as tapered single-mode fiber [7,8], or tapered multimode fiber [9,10], and some tapered sensors can increase their sensitivity by nanofilm enhancement [11–13]. Other types of RI sensor such as a Fabry-Perot based fiber optic interferometer [14–16], a fiber Bragg grating (FBG) [17,18], a singlemode-multimode-singlemode (SMS) fiber structure [19–21]. The underlying operating principle of sensors based on SMS structure is multimode interference excited between modes in the multimode fiber (MMF). Despite popularity and high sensitivity, these sensors are stringent fiber fabrication process and the cost are very high due to the use of expensive metal film.

Recently, multicore fiber have shown great potential for sensing applications, like strain [22], curvature [23], temperature [24], and shape sensing [25]. In this paper, we proposed and experimentally demonstrated a novel RI sensor based on an middle-tapered multicore fiber, which simply spliced between two single mode fibers and can be described as SMF-TMCF-SMF structure. The shift in the transmission spectrum depends on the surrounding refractive index solution in the multicore fiber region. And the transmission of the TMCF showing sensitivity to external refractive index, which makes it possible to be an RI sensor. This simple RI sensor structure may suitable for realizing simultaneous multi-parameter measurement with MCF. In addition, we also simulated the sensitivity of cladding mode with different external RI.

2. Working principle

In a SMF28-MCF-SMF28 fiber structure, as shown in Fig. 1.

Interference between these multiple modes within the MCF occurs and dictates the output spectral response of the SMS fiber structure, which is thus affected by the surrounding liquid RI.

In a SMF-TMCF-SMF fiber structure, cladding modes high order modes are excited within the cladding of the MCF section because of the core mismatch between SMF28 and MCF, and the excited modes would travel along the four cores and then are back into the core of SMF-28. It's worth noting that the light also conduct in the four core, however here external refractive index main influencing cladding mode, so we mainly research the change of the cladding mode. Multimode interference for these cladding modes occurs within the MCF section. It is well known that the propagation constant of the cladding mode (corresponding to effective RI) is influenced by the RI of the surrounding environment. Thus, the relative phase difference between two interfering modes can be expressed by,

$$\Delta\varnothing = \frac{2\pi}{\lambda}(\Delta n)L \tag{1}$$

* Corresponding author.
E-mail address: lijing@bjtu.edu.cn (J. Li).

http://dx.doi.org/10.1016/j.yofte.2016.11.008
1068-5200/

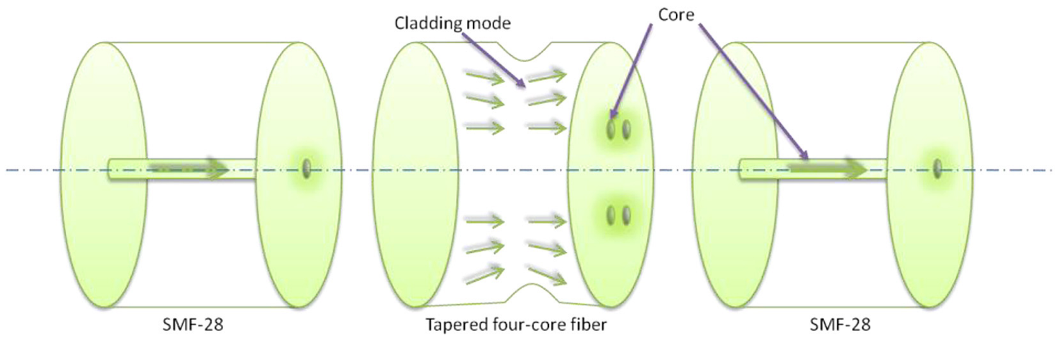

Fig. 1. Schematic diagram of SMF-TMCF-SMF structure with four core fiber.

where λ is the wavelength of the light source, L is the length of the MCF, and Δn is the effective refractive index difference, which can be expressed as,

$$\Delta n = n_{eff}^{co} - n_{eff}^{ou} \tag{2}$$

where n_{eff}^{co} is the effective refractive indices of core mode and n_{eff}^{ou} is the effective refractive indices of higher order modes out of the core.

Assuming that the SMF and MCF are ideally aligned, due to the circular symmetry of the input field, only LP_{0m} modes will be excited in the MCF when light travels from SMF to MCF. If the input light in the SMF has a fundamental mode field distribution $E_1(r)$, then the input field can be decomposed into the eigenmodes LP_{0m} in the MCF when the light enters the MCF section. The field MCF section at a propagation distance L can be described by,

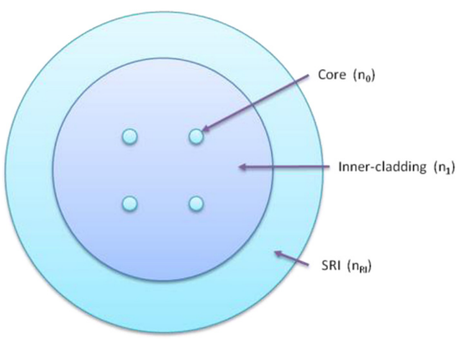

Fig. 2. Configuration of MCF model structure with double-cladding.

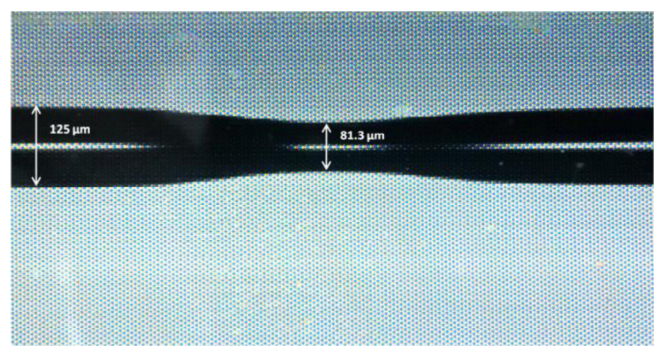

Fig. 4. The picture of tapered MCF.

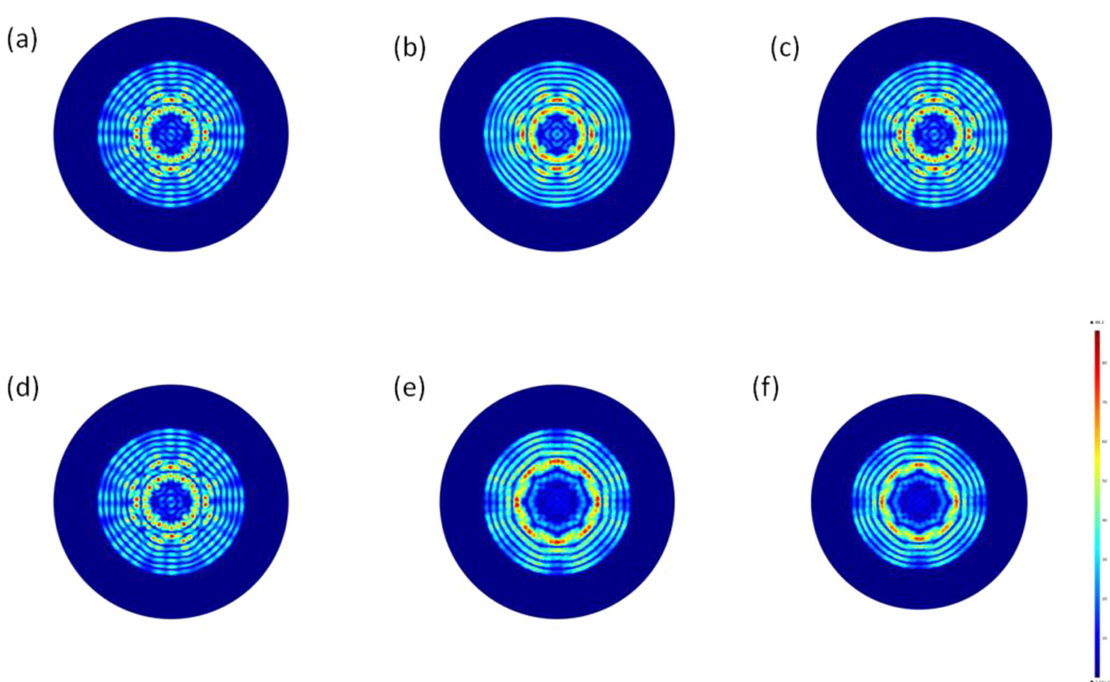

Fig. 3. Mode field distribution for inner cladding are obtained by using FEM with different SRI: (a) 1.33, (b) 1.34, (c) 1.35, (d) 1.36, (e) 1.37, (f) 1.38.

$$E(r, L) = \sum_m \eta_m E_1(r) \exp(j\beta_m L) \quad (3)$$

where β_m is the propagation constant. L is the length of TMCF, and η_m is the excitation coefficient of each mode.

We simulated that how the RI change affect the multimode interference by using full vector finite element method (FEM).

As shown in Fig. 2, we create a multicore fiber model with double-cladding, and we can observed that the mode field

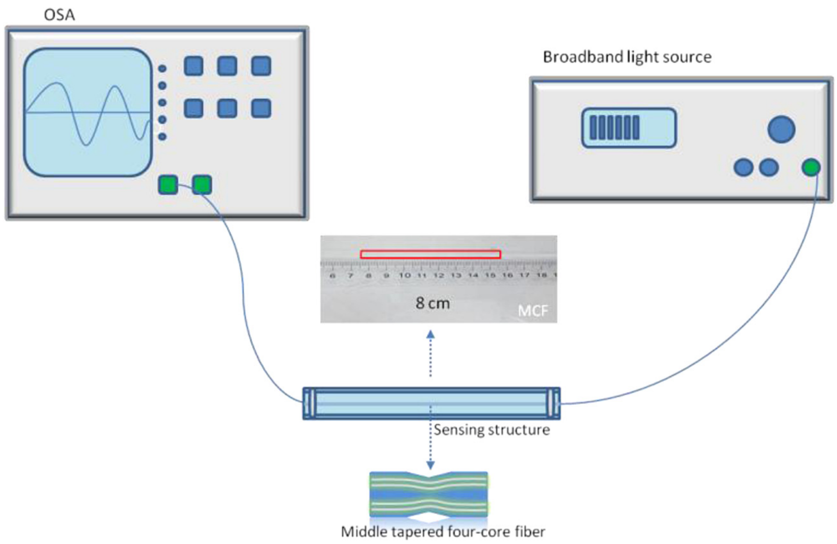

Fig. 5. Experimental setup for the RI sensing.

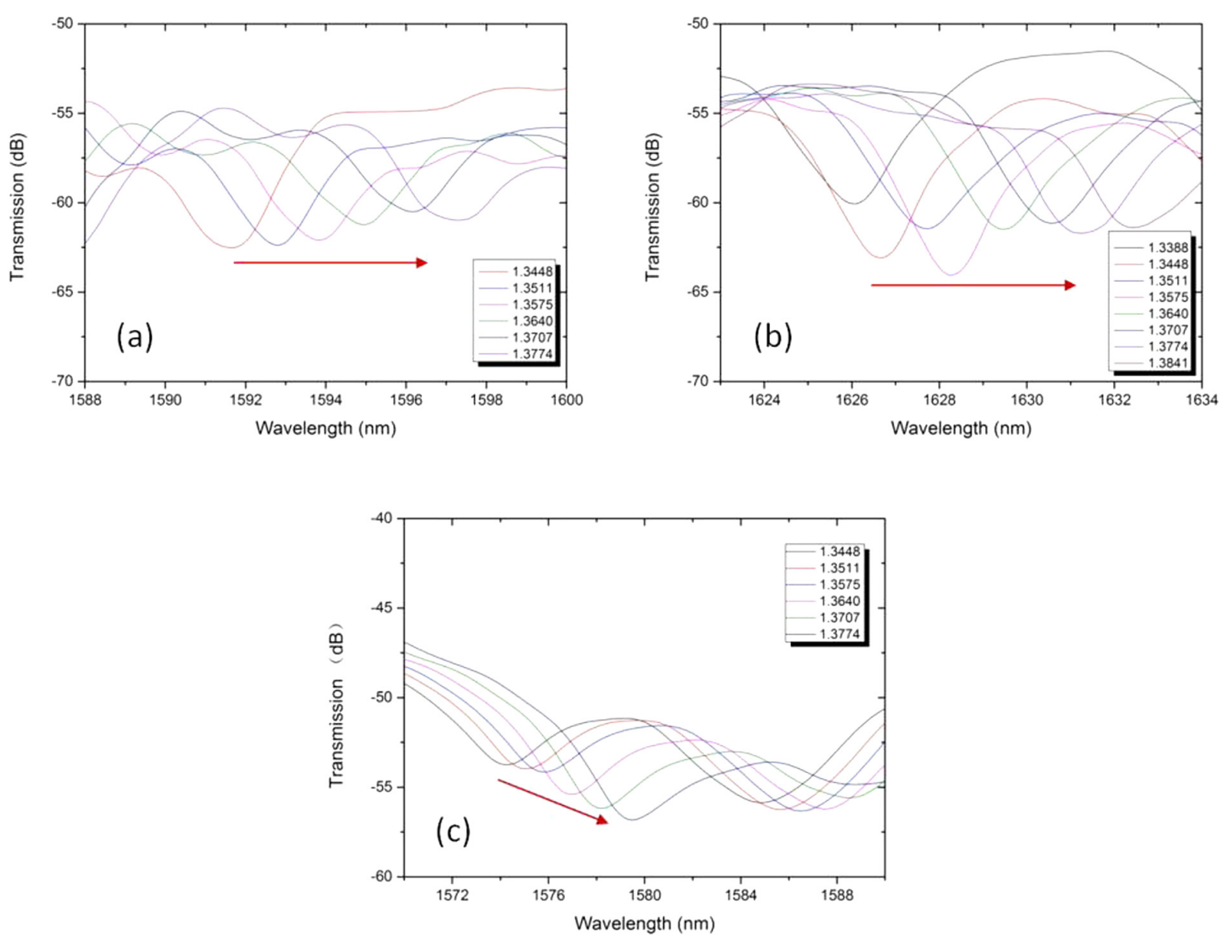

Fig. 6. Measured spectral response of structure L-17 and L-8, at different SRI. (a) wavelength ranging from 1591.62 to 1597.22 nm (L-17) with the RI ranges:1.3448–1.3774 and (b) wavelength ranging from 1626.02 to 1632.42 nm (L-17) with the RI ranges:1.3388–1.3841. (c) wavelength ranging from 1574.24 to 1579.45 nm (L-8) with the RI ranges: 1.3448–1.3774.

distribution of inner cladding is changing with different refractive indices of outer cladding, as shown in Fig. 3. It is worth saying that we calculated the mode field distribution at 1550 nm, and the effective refractive index range of second cladding changing from 1.33 to 1.38.

As we can see in Fig. 3, when the effective RI of second cladding changing from 1.33 to 1.38, the mode field distributions of cladding have a corresponding change. Therefore, a change in the SRI for the sensor will affect the multimode interference, and in turn $\Delta\varnothing$ (based on Eq. (1)) changes, this will result in changes in the spectral response which can be monitored by an optical spectrum analyzer (OSA).

3. Fabrication and setup

A simple, non-tapered MCF structure with a relatively large diameter (125 μm), resulting in a relatively small portion of the evanescent field being in contact with the surrounding environment, and, hence, such a sensor may has relatively low sensitivity. In this letter we pulling the multicore fiber while heating, that the diameter of the fiber at this region is less than the original diameter. Then, the portion of the evanescent field exposed to the surrounding environment is increasing, which will increase the sensitivity of the sensor.

In our experiments, a section of MCF with length of circa 17 cm and 8 cm respectively fusion spliced between two SMF-28 fibers. And it is noted that the MCF section was tapered in the middle position using taper program. Two sensor samples were fabricated with tapered waist diameters (81.3 and 75.9 μm). The waist diameter was measured in fusion splitter's window by the relative proportions as shown in Fig 4. The prepared sensor samples are referred hereinafter to as L-17, L-8. For each sample, the taper waist length for L-17, L-8 are circa 0.56 mm and 0.64 mm, respectively.

The schematic diagram of the RI measuring system and a tapered fiber structure is shown in Fig. 5. The SMS is fabricated by a commercial fusion splicer (Ericson, Fsu-975). One piece of MCF (FIBERCORE, SM-4C 8.0/125) is removed jacket and the fiber end faces are cleaned by fiber cleaver (Furukawa, S325). The MCF and a prepared SMF are putted on the splicer and adjusted to alignment. Light from a broadband light source (KOHERAS, SuperK Uersa) 1450–1650 nm is launched into the tapered S-M-S structure, while the transmitted light is measured by an OSA (YOKOGAWA AQ6375) with resolution bandwidth set at 0.05 nm. The RI liquid can be placed on the glass slide so that the tapered MCF fiber section is immersed in the liquid, and ensuring that the fiber sensor was always straight and the sensing section was slightly above the slide to avoid any physical contact with the glass surface. It is worth mentioning that all the tests were conducted at room temperature.

For RI measurement, we have prepared series RI liquid samples for the measurement. The corresponding RIs are 1.3388, 1.3448, 1.3511, 1.3575, 1.3640, 1.3707, 1.3774, and 1.3841. For each measurement, a small quantity of the solution is dropped into

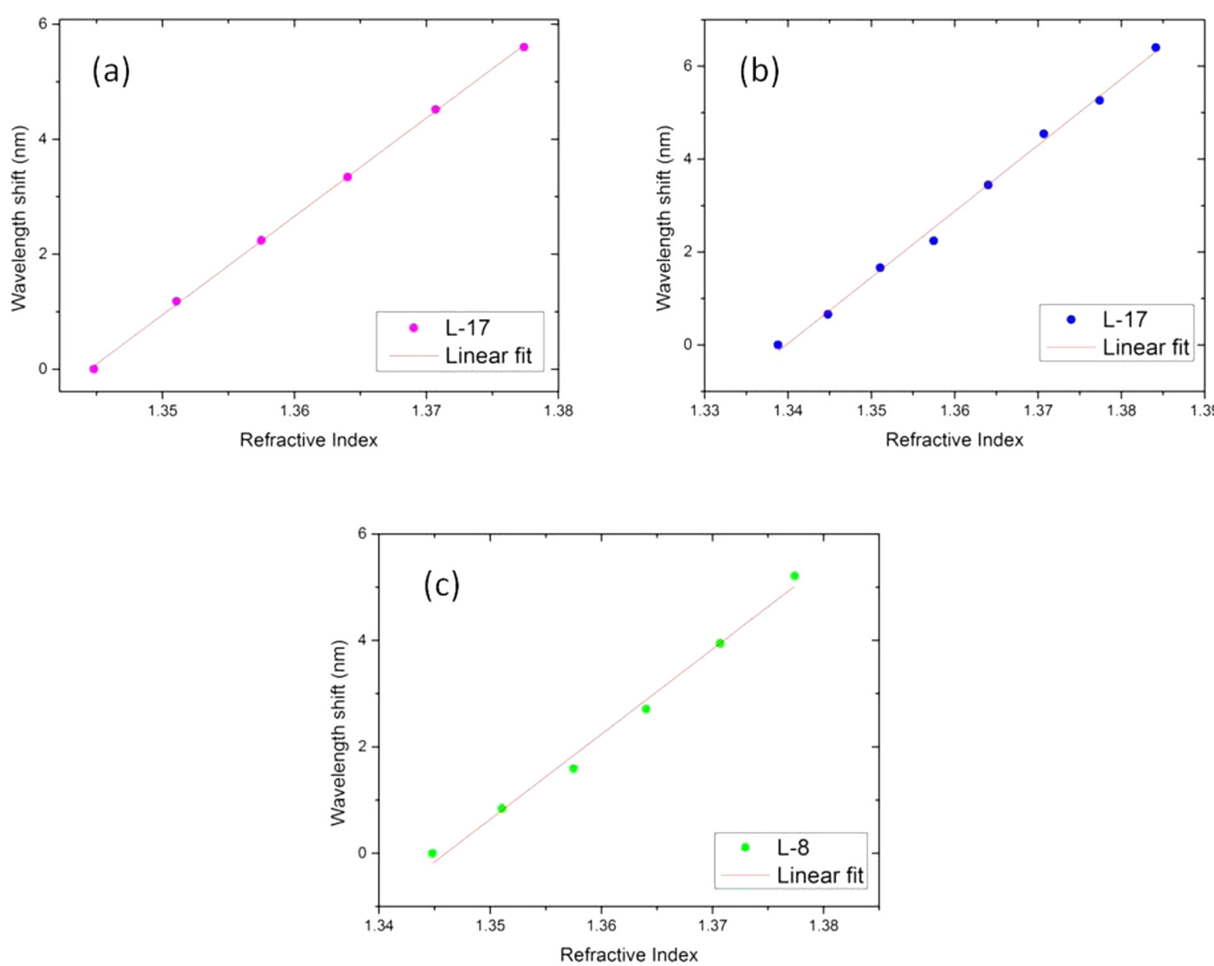

Fig. 7. Measured spectral wavelength shift versus RI for different sensors.

Table 1
Sensor sensitivities and linear fit correlative coefficient.

Sensors	L-17	L-17	L-8
	(1591.62–1597.22 nm)	(1626.02–1632.42 nm)	(1574.24–1579.45 nm)
RI Range	1.3448–1.3774	1.3388–1.3841	1.3448–1.3774
Linear fit correlative coefficient	0.9995	0.9955	0.9893
Sensitivity (nm/RIU)	171.2	142.4	159.8

the U-shape groove until the sensing element is fully immersed. After the measurement, the sensor is cleaned with deionized water and dried in air.

4. Results and discussion

Fig. 7(a) and (b) shows two different range of the measured spectral responses for the L-17 sensor, and Fig. 7(c) shows spectral responses for the L-8 sensor. The RI value ranges are (a) 1.3448–1.3774, (b) 1.3388–1.3841, (c) 1.3448–1.3774. It can be observed that the wavelength of the spectral dip moves monotonically toward longer wavelengths as the SRI increases in every case. When the RI changes from 1.3448 to 1.3774 and 1.3388 to 1.3841, the wavelengths of the dips shift about 5.6 nm, 6.4 nm and 5.2 nm for L-17(1591.62 nm-1597.22 nm), L-17(1626.02 nm-1632.42 nm) and L-8(1574.24 nm-1579.45 nm), respectively. The L-17 sensor as shown in Fig. 7(a) and (b) and L-8 sensor as shown in Fig. 7(c) have different spectral responses, but the direction of the wavelength shift with increasing SRI is the same.

The dip wavelength shifts versus RI change for the sensors are presented in Figs. 6 and 7 and summarized in detail in Table 1. As expected, RI sensitivity increases as the length of the sensor section(here refer to MCF) increases. This is likely because of the fact that long sensors have a larger portion of the evanescent field exposed to the surrounding environment.

As shown in Table 1, for all three samples, the linear correlative coefficients R^2 are greater than 0.989, which indicates that the wavelength shift exhibits good linear relationship with the RI change over a small RI range. The sensitivities for L-17(1591.62–1597.22 nm), L-17(1626.02–1632.42 nm)and L-8(1574.24–1579.45 nm) are 171.2 nm/RIU (RI 1.3448–1.3774), 142 nm/RIU (RI 1.3388–1.3841), and 159.8 nm/RIU (RI 1.3448–1.3774), respectively. Taking into account that the OSA has a wavelength resolution of 0.05 nm, the RI sensor based on L-17(1591.62 nm–1597.22 nm) has an RI resolution of 2.92×10^{-4} RIU.

Although the sensitivity of proposed sensor is not very high, but it can be combined with a relatively high sensitivity RI sensor. The lower sensitivity RI sensor used to determine the approximate RI range of the analyte, and applied appropriate sensor to measuring a highly accurate RI value for the analyte. Moreover, the multi-core optical fiber sensor can be used to realizing simultaneous multi-parameter measurement.

5. Conclusion

In conclusion, we developed a simple RI sensor based on SMF-TMCF-SMF structure.

By employing the middle-tapered optical multicore fiber in the sensing section, a sensitive ambient RI detection could be realized over the RI range from 1.345 to 1.377. We compared and analyzed sensing performance with different lengths of sensor structure. A good interference spectrum with the extinction ratio of as much as 10 dB was obtained and a sensitivity of 171 nm/RIU was achieved with 17 cm length TMCF. This simple RI sensor structure may suitable for realizing simultaneous multi-parameter measurement with MCF. Furthermore, by decreasing the diameter of MCF section, the sensitivity can be improve to meet more application scenarios, like chemical sensing or bio-sensing.

Acknowledgment

This work is jointly supported by the National Natural Science Foundation of China (61525501).

References

[1] C.K.Y. Leung, K.T. Wan, D. Inaudi, X. Bao, W. Habel, Z. Zhou, J. Ou, M. Ghandehari, H.C. Wu, M. Imai, Review: optical fiber sensors for civil engineering applications, Mater. Struct. 48 (2013) 871–906.
[2] S. Liehr, P. Lenke, M. Wendt, K. Krebber, M. Seeger, E. Thiele, H. Metschies, B. Gebreselassie, J.C. Munich, Polymer optical fiber sensors for distributed strain measurement and application in structural health monitoring, IEEE Sens. J. 9 (2009) 1330–1338.
[3] D. Barrera, V. Finazzi, J. Villatoro, S. Sales, V. Pruneri, Packaged optical sensors based on regenerated fiber Bragg gratings for high temperature applications, IEEE Sens. J. 12 (2012) 107–112.
[4] Z. Yin, Y. Geng, X. Li, X. Tan, R. Gao, V-groove all-fiber core-cladding intermodal interferometer for high-temperature sensing, Appl. Opt. 54 (2015) 319–323.
[5] G. Tsiminis, T.S. Klari'c, E.P. Schartner, S.C. Warren-Smith, M.D. Lewis, S.A. Koblar, T.M. Monro, Generating and measuring photochemical changes inside the brain using optical fibers:exploring stroke, Biomed. Opt. Express 5 (2014) 3975–3980.
[6] T.K. Yadav, R. Narayanaswamy, M.H. Abu Bakar, Y.M. Kamil, M.A. Mahdi, Single mode tapered fiber-optic interferometer based refractive index sensor and its application to protein sensing, Opt. Express 22 (2014) 22802–22807.
[7] Y. Zhao, X.-G. Li, L. Cai, A highly sensitive Mach-Zehnder interferometric refractive index sensor based on core-offset single mode fiber, Sens. Actuators A (2015) 119–124.
[8] P. Wang, G. Brambilla, M. Ding, Y. Semenova, Q. Wu, G. Farrell, High-sensitivity, evanescent field refractometric sensor based on a tapered, multimode fiber interference, Opt. Lett. 36 (2011) 2233–2235.
[9] M.I. Zibaii, A. Kazemi, H. Latifi, M.K. Azar, S.M. Hosseini, M.H. Ghezelaiagh, Measuring bacterial growth by refractive index tapered fiber optic biosensor, J. Photochem. Photobiol. B 101 (2010) 313–320.
[10] S. Zhu, F. Pang, S. Huang, F. Zou, Y. Dong, T. Wang, High sensitivity refractive index sensor based on adiabatic tapered optical fiber deposited with nanofilm by ALD, Opt. Express 23 (2015) 13880–13888.
[11] Y. Zhao, F. Pang, Y. Dong, J. Wen, Z. Chen, T. Wang, Refractive index sensitivity enhancement of optical fiber cladding mode by depositing nanofilm via ALD technology, Opt. Express 21 (2013) 26136–26143.
[12] A. Shabaneh, S. Girei, P. Arasu, M. Mahdi, S. Rashid, S. Paiman, M. Yaacob, Dynamic response of tapered optical multimode fiber coated with carbon nanotubes for ethanol sensing application, Sensors 15 (2015) 10452–10464.
[13] C.R. Biazoli, S. Silva, M.A. Franco, O. Frazão, C. Cordeiro, Multimode interference tapered fiber refractive index sensors, Appl. Opt. 51 (2012) 5941–5945.
[14] J.N. Dash, R. Jha, Fabry-Perot based strain insensitive photonic crystal fiber modal interferometer for inline sensing of refractive index and temperature, Appl. Opt. 54 (2015) 10479–10486.
[15] B. Dong, J. Hao, T. Zhang, J.L. Lim, High sensitive fiber-optic liquid refractive index tip sensor based on a simple inline hollow glass micro-sphere, Sens. Actuators B (2012) 405–408.
[16] C.R. Liao, T.Y. Hu, D.N. Wang, Optical fiber Fabry-Perot interferometer cavity fabricated by femtosecond laser micromachining and fusion splicing for refractive index sensing, Opt. Express 20 (2012) 22813–22818.
[17] T. Guo, H.-Y. Tam, P.A. Krug, J. Albert, Reflective tilted fiber Bragg grating refractometer based on strong cladding to core recoupling, Opt. Express 17 (2009) 5736–5742.
[18] B. Gu, W. Qi, J. Zheng, Y. Zhou, P.P. Shum, F. Luan, Simple and compact reflective refractometer based on tilted fiber Bragg grating inscribed in thin-core fiber, Opt. Lett. 39 (2014) 22–25.
[19] Q. Wu, Y. Semenova, P. Wang, G. Farrell, High sensitivity SMS fiber structure based refractometer–analysis and experiment, Opt. Express 19 (2011) 7937–7944.
[20] L.-L. Xue, L. Yang, Sensitivity enhancement of RI sensor based on SMS fiber structure with high refractive index overlay, J. Lightwave Technol. 30 (2012) 1463–1469.

[21] Y. Zhao, L. Cai, X.-G. Li, F.-C. Meng, Z. Zhao, Investigation of the high sensitivity RI sensor based on SMS fiber structure, Sens. Actuators A (2014) 186–190.
[22] Y. Mizuno, N. Hayashi, H. Tanaka, Y. Wada, K. Nakamura, Brillouin scattering in multi-core optical fibers for sensing applications, Sci. Rep. 5 (2015) 11388.
[23] G. Salceda-Delgado, A. Van Newkirk, J.E. Antonio-Lopez, A. Martinez-Rios, A. Schülzgen, R.A. Correa, Compact fiber-optic curvature sensor based on super-mode interference in a seven-core fiber, Opt. Lett. 40 (2015) 1468–1471.
[24] J.E. Antonio-Lopez, Z.S. Eznaveh, P. LiKamWa, A. SchÜlzgen, R. Amezcua-Correa, Multicore fiber sensor for high-temperature applications up to 1000 °C, Opt. Lett. (2014) 4309–4312, Optical Society of America.
[25] J.P. Moore, M.D. Rogge, Shape sensing using multi-core fiber optic cable and parametric curve solutions, Opt. Express 20 (2012) 2967–2973.